Progress In Electromagnetics Research M, Vol. 118, 1–10, 2023

Research and Design of a Dual-Band Reflective Focused Metasurface for Wireless Power Transfer

Bo Yin, Zhu Xu*, Junhao Cong, Xiangdong Fu, Haibin Xu, and Zhuoze Wu

Abstract—To solve the problem of single working frequency of traditional reflective focused metasurface, a dual-band reflective focused metasurface is proposed, which can realize independent focusing characteristics at 7.25 GHz and 20.5 GHz. The metasurface unit is composed of metal elements combined by a split-ring resonant structure working at 7.25 GHz and an elliptical resonant structure working at 20.5 GHz in the same plane, dielectric substrate, and ground. Dual-band independent control and 360° phase coverage are achieved by adjusting the dimensions of unit. The surface current distribution also verifies the rationality of the designed metasurface element. Based on the principle of quasi-optical path, a dual-band reflective focused metasurface with independent focusing characteristics is designed. Through full-wave simulation, the focusing efficiency at 7.25 GHz and 20.5 GHz is calculated by Poynting theorem, which are 56.9% and 57.5%, respectively. The proposed dual-band metasurface has the characteristics of simple structure and low profile without multi-layer stacking and metal through-holes.

1. INTRODUCTION

Near-field focusing (NFF) transmission technology is widely used in many aspects, such as optical imaging [1], wireless power transfer (WPT) [2], and radio frequency identification (RFID) [3]. NFF is a characteristic of Fresnel and near-field regions of antennas [4, 5]. Theoretically, electromagnetic waves from the transmitting source can be focused at a certain point in near-field region within the boundary $2D^2/\lambda$. Since the last century, NFF has been realized through various antenna structures, such as parabolic reflector [6], dielectric lens antenna [7], microstrip phased array [8–11], and planar Fresnel zone plate [12, 13]. However, the development of NFF in a WPT system has been hindered because of the high cost of processing parabolic reflectors, the complexity of microstrip array feeding, and the low efficiency of planar Fresnel zone plate lens. Therefore, WPT system needs more diversity and flexibility in actual applications. Therefore, it has attracted researchers' attention to better controlling the focusing beam.

In recent years, metasurface technology has provided a new way for electromagnetic wave regulation, which has attracted the attention of more and more scholars all over the world [14]. By adjusting the orientation angle and size of each metasurface element, the phase of scattered wave can be controlled in space to shape the wavefront [15–17]. Based on this concept, it is easier to realize NFF. Furthermore, metasurface has the advantages of light weight, low profile, and simple structure, which is more practical. In [18], Chia et al. designed a one-dimensional reflective focusing metasurface with a central frequency of 5.8 GHz using a horn antenna as feeding source, and the reflected wave is focused at 10 to 12 operating wavelength away from the metasurface array. In [19], Zhang et al. designed a cross dipole element array, which uses a horn antenna as the feeding source to focus in near-field. And the array can generate

Received 6 March 2023, Accepted 15 May 2023, Scheduled 5 July 2023
* Corresponding author: Zhu Xu (1826113722@qq.com).
The authors are with the School of Optoelectronic Engineering, Chongqing University of Posts and Telecommunications, Chongqing 400065, China.

focal points at different positions by making use of the polarization independence of its elements, in which the maximum focusing efficiency of a single focal point can reach 65.9% [16]. However, their operating frequency band is limited to a single frequency band, which limits the application of NFF technology in WPT system to a certain extent. In [20], Zhang et al. proposed a double-layer coding metasurface of embedded PIN diode. By changing the coding mode of the units on the upper and lower plane, the focal length can be dynamically varied from 100 mm to 150 mm and 200 mm to 300 mm at 6 GHz and 9.8 GHz, respectively, which improved the freedom of NFF technology in WPT system. A dual-band reflective metasurface operating at 5.8 GHz and 10 GHz is proposed in [21]. Based on the dual polarization independent control structure unit, the NFF beams with different polarizations are obtained. The simulation results show that the near-field focusing characteristics are better than the Bessel beam under the same conditions.

In this paper, a reflective metasurface array for NFF is proposed. A novel sing-layer dual-band metasurface unit is proposed to realize dual-band focusing. For both 7.25 GHz and 20.5 GHz, the reflection phase shift of the proposed unit can achieve about 360°. And the reflection phase at corresponding frequencies can be independently controlled respectively. Then a reflective metasurface with a single near-field focus using 15 × 15 elements with the size of 210 mm × 210 mm is designed. Finally, NFF is achieved at 7.25 GHz and 20.5 GHz by vertically irradiating the metasurface using circularly polarized plane wave as the source.

2. METASURFACE ELEMENT DESIGN

The metasurface element proposed in this paper is shown in Figure 1. As depicted, it comprises monopole and split-ring resonant structures, working at 15.25 GHz and 7.25 GHz respectively, a metallic square ground plane, and a Polyimide substrate with a relative permittivity of 3.5 between them. The thickness of substrate is $h = 2$ mm. After optimization design, other parameters are selected as follows: $P = 14$ mm, $R_1 = 6.25$ mm, $R_2 = 5.55$ mm, $L = 5$ mm, $W = 0.5$ mm, $\alpha_1 = 350°$. Moreover, α_2 and α_3 are the orientation angles of the monopole and split-ring structures towards y-axis, respectively.

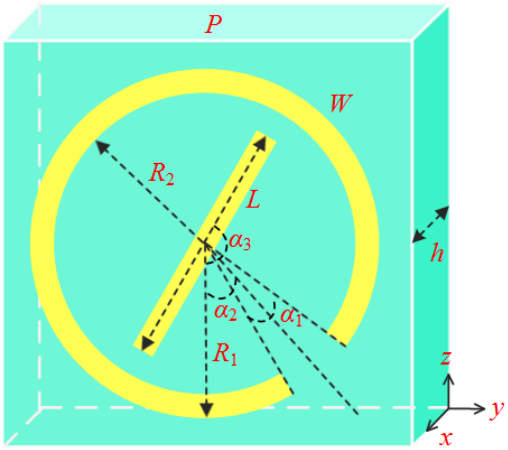

Figure 1. The geometric structure of metasurface element.

To estimate the performance of the proposed metasurface element, a full-wave period simulation is applied using CST Microwave studio. As shown in Figure 2, when α_2 and α_3 vary from 0° to 180°, the amplitude of reflective wave at 15.25 GHz and 7.25 GHz remains constant at over 0.9, meeting the requirement of focusing metasurface element. In addition, it can be found that when the rotation angle of the split-ring resonant structure changes from 0° to 180°, the reflection phase shift of the metasurface element at 7.25 GHz is about 360° as shown in Figure 3(a). By contrast, big fluctuation at 15.25 GHz can be found in this situation, which is 66.04°. So, this phenomenon indicates that the coupling between the two small structures is strong and does not meet the design requirements of dual-band structure.

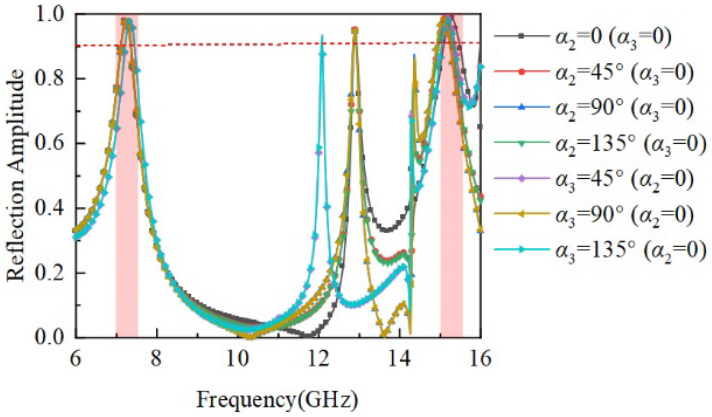

Figure 2. Reflection amplitude of the dual-band metasurface element.

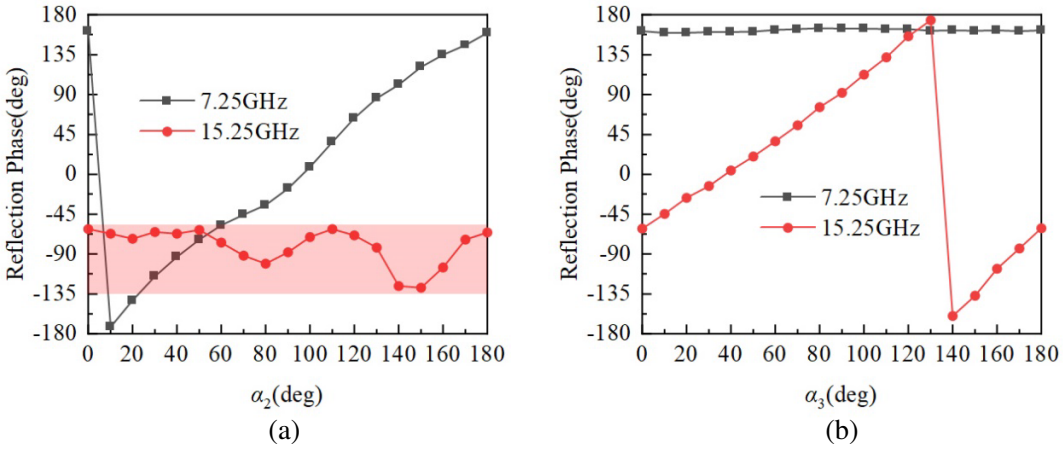

Figure 3. Reflection phase of the dual-band metasurface element. (a) Reflection phase versus the orientation angle α_2 of the split-ring structure. (b) Reflection phase versus the orientation angle α_3 of the monopole structure.

In Figure 3(b), small fluctuation of the reflection phase can be found at 7.25 GHz when the orientation angle of the monopole structure changes from 0° to 180°. By comparison, the reflection phase at 15.25 GHz spans about 360° in the same situation.

After many modifications, the previous monopole resonant structure is replaced by ellipse-ring resonant structure, and other structures remain unchanged. The structural parameters of the optimized elliptical structure are $a = 5$ mm, $b = 1$ mm, as shown in Figure 4.

As displayed in Figure 5, the amplitude of reflected wave at 20.5 GHz and 7.25 GHz remains constant with the dual resonant restructure by an angle ranging from 0° to 180°, and it is both greater than 0.9. At the same time, it can be found that the reflection phase shift of the metasurface element at 7.25 GHz is about 360° in Figure 6(a) when the orientation angle of the split-ring resonant structure changes from 0° to 180°. In addition, there is a small fluctuation in the reflection phase of the metasurface element at 20.5 GHz. In this case, a similar phenomenon can be found in Figure 6(b). Hence, it can be concluded that the reflection phase at 7.25 GHz and 20.5 GHz can be independently controlled by changing the orientation angle of elliptical and split-ring resonant structure respectively. To sum up, compared with the previous metasurface element structure, the reflection amplitude of the optimized metasurface element is slightly higher, but the fluctuation of the reflection phase is smaller. And the optimized metasurface element has a larger span of dual operating frequency, which has better practical application. So the optimized metasurface element has better dual-band feature.

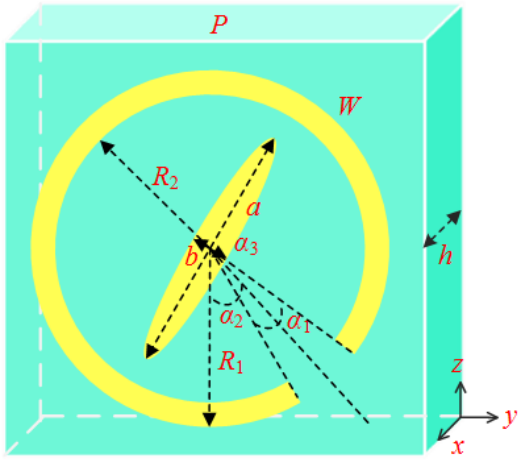

Figure 4. The schematic of optimized metasurface element.

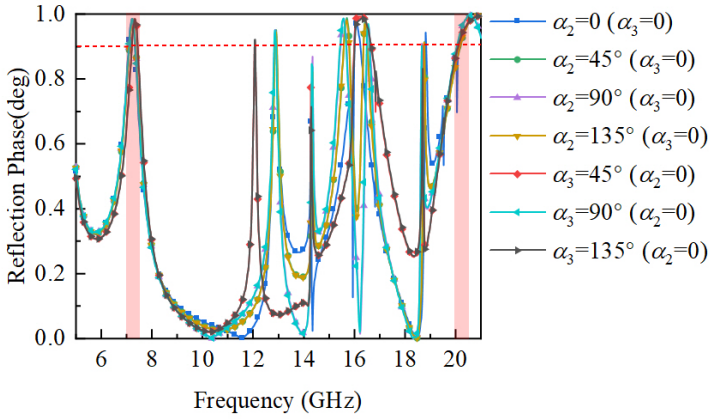

Figure 5. Reflection amplitude of the optimized dual-band metasurface element.

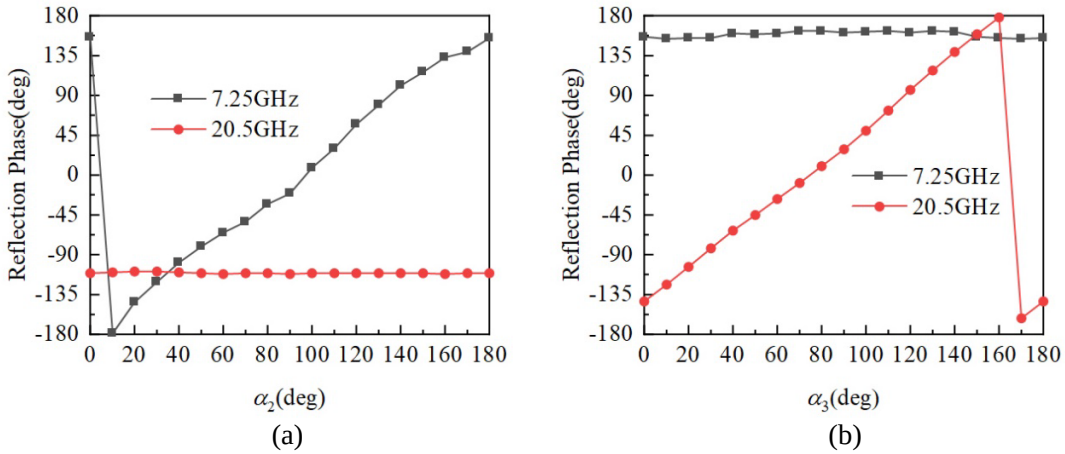

Figure 6. Reflection phase of the optimized dual-band metasurface element. (a) Reflection phase versus the orientation angle α_2 of the split-ring structure. (b) Reflection phase versus the orientation angle α_3 of the elliptical structure.

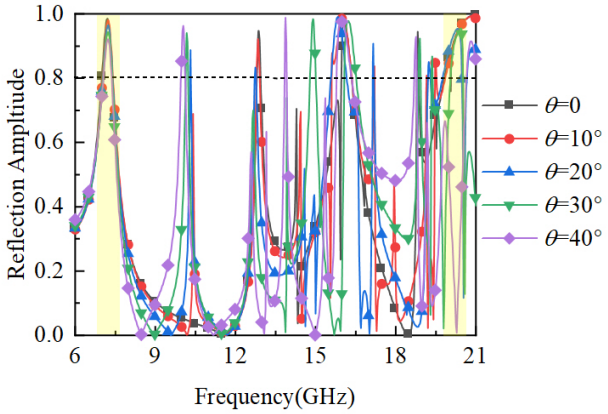

Figure 7. Reflection amplitude of metasurface unit at oblique incidence.

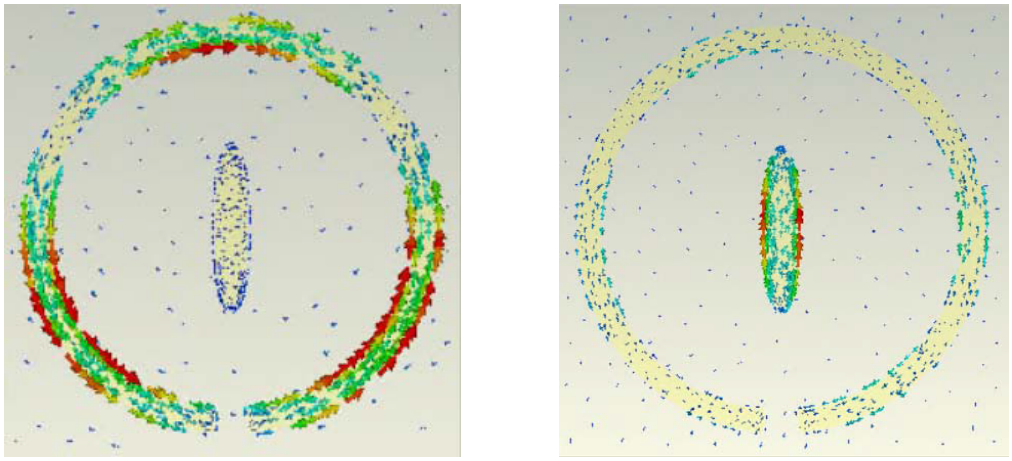

(a) (b)

Figure 8. Current distribution diagram of metasurface unit. (a) Current distribution diagram of metasurface unit at 7.25 GHz. (b) Current distribution diagram of metasurface unit at 20.5 GHz.

At the same time, in practical applications, electromagnetic waves radiating on a focused metasurface may not incident perpendicular to surface. So, it is necessary to discuss the focusing performance of metasurface unit at oblique incidence. The simulation results are shown in Figure 7, and it can be seen that as the incident angle increases, high reflection can still be maintained at 7.25 GHz and 20.5 GHz. However, as the incident angle further increases, the reflection amplitude at 20.5 GHz has decreased, indicating that the incident angle has a significant influence on reflection amplitude at high frequency. However, the designed metasurface unit can maintain good reflection from 0 to 30°, which basically meets the requirements for dual-band metasurface unit.

Finally, H-field and surface current monitor at 7.25 GHz and 20.5 GHz is added to observe the proposed dual-band metasurface unit, and the corresponding current distribution diagram is shown in Figure 8. It can be observed that the surface current distribution of split-ring structure at 7.25 GHz is concentrated, and the current intensity is large, while the current intensity of elliptical structure is small in Figure 8(a). At the same time, it can be observed that the surface current distribution of split-ring structure at 20.5 GHz is sparse, and the current intensity is small, while the current distribution of elliptical structure is dense, and the current intensity is large in Figure 8(b). This phenomenon shows that the coupling between split-ring structure and elliptical structure is small, which meets the design requirements of dual-band metasurface and is consistent with the analysis of reflection phase parameters in Figure 6.

3. DESIGN ON NFF METASURFACE

3.1. Near-Field Focused Metasurface Design

The phase distribution of the reflective metasurface is determined by the operating frequency of incident wave, excitation mode, focus position, and other indicators. As shown in Figure 9, the reflecting surface is located in the xoy plane, with the geometric center of the whole reflecting surface as the coordinate origin, and the plane wave is illuminated from above the xoy plane. Each metal unit structure on the reflecting surface can be regarded as a point source, and the central coordinate of the metal unit structure can be used as the coordinate of the point source, so as to independently adjust the reflection phase of the units at different positions on the front of the reflecting electromagnetic surface, and different focusing functions can be obtained. Based on the superposition principle of fields, the electric field distribution required to generate multiple focal points can be obtained by adding the electric field vectors required to generate each independent focal point. Assuming that there are n focal points at different positions, the aperture field distribution of the whole reflecting surface can be expressed as

$$E_R(x_i, y_i) = A(x_i, y_i)e^{j\varphi(x_i,y_i)} = \sum_{n=1}^{N} A_n(x_i, y_i)e^{j\varphi_i(x_i,y_i)}, \tag{1}$$

where (x_i, y_i) is the coordinate of the center position of the ith element, and $A_n(x_i, y_i)$ and $\varphi_n(x_i, y_i)$ are the required amplitude and phase of the ith element to generate the nth focus on the reflective plane. Therefore, $A(x_i, y_i)$ and $\varphi(x_i, y_i)$ are the final amplitude and phase information to generate the ith element of the nth focus.

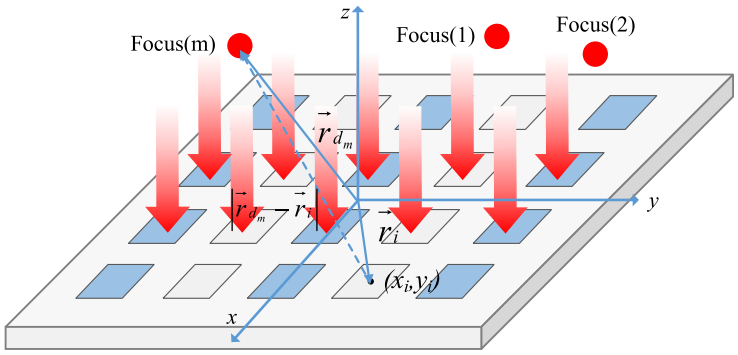

Figure 9. The diagram of NFF metasurface.

Using the plane wave of vertical incidence as the feeding source, only the phase information caused by the path difference from the focus point to the metasurface needs to be considered. According to the electromagnetic wave propagation theory, the phase is equal to the multiplication of wave number and wave path, and the distance between each element on the reflective metasurface and the focus position is $|\vec{r}_{d_m} - \vec{r}_i|$, so

$$\Delta\varphi_i(x_i, y_i) = \varphi_d(x_i, y_i) \tag{2}$$

the final phase shift on the ith element can be obtained as follows:

$$\varphi_d(x_i, y_i) = k\,|\vec{r}_{d_m} - \vec{r}_i| \tag{3}$$

3.2. Simulation Results

Through literature review, it can be found that the ratio of focal length and the size of metasurface array is greater than 1, as shown in Table 1. Therefore, the design goal of this paper is to focus at a distance of 220 mm from the super surface, that is, the focal length $F = 220$ mm. In practical applications, the beam needs to focus flexibly in near field, and the shielding effect of the feed on the reflected wave should be avoided. Based on the theory in Section 1, the reflective phase distribution of metasurface is calculated through MATLAB in Figure 10. The working frequencies of the reflective metasurface are 7.25 GHz and 20.5 GHz, and the metasurface is composed of 15×15 elements.

Table 1. The comparison of reflective metasurface.

Reference	Focal distance/mm	Metasurface's aperture length/mm	Ratio
[19]	1000	390	2.56
[22]	1000	520	1.92
[23]	500	405	1.23
This paper	220	210	1.05

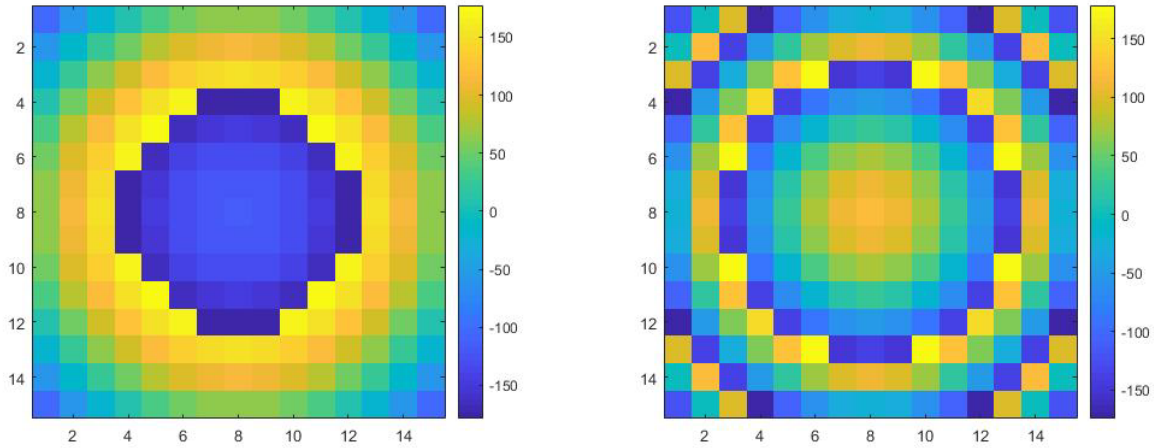

Figure 10. Metasurface compensated phase distribution. (a) 7.25 GHz, (b) 20.5 GHz.

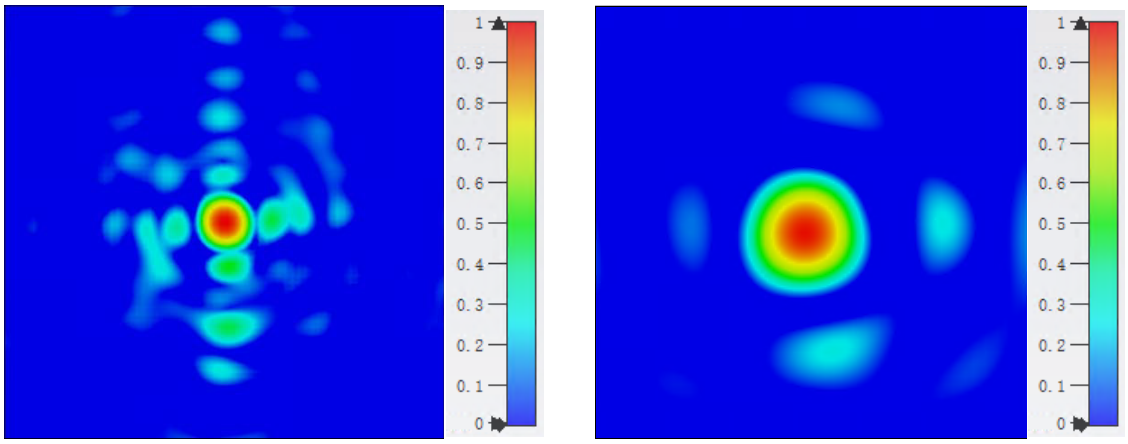

Figure 11. The normalized electric field distribution at $z = 220\,\text{mm}$. (a) 7.25 GHz, (b) 20.5 GHz.

When the circularly polarized plane wave irradiates the metasurface array vertically, taking the position $z = 220\,\text{mm}$ and the size $210\,\text{mm} \times 210\,\text{mm}$ in the simulation results, the distributions of normalized electric field intensity on the xoy plane are shown in Figure 11(a) and Figure 11(b). Among them, the maximum positions of field intensity at 7.25 GHz and 20.5 GHz are $(-1.75, -5.07, 220)\,\text{mm}$ and $(1.62, -1.65, 220)\,\text{mm}$ respectively, which are consistent with the ideal focusing position $(0, 0, 220)\,\text{mm}$. At the same time, the distribution characteristics of electric field intensity in the plane of are relatively consistent with the expected distribution characteristics.

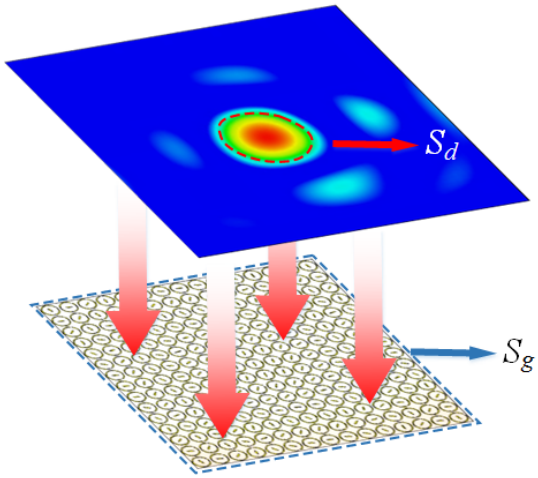

Figure 12. The schematic of focusing efficiency calculation.

4. ANALYSIS OF NFF EFFICIENCY

How to analyze and calculate the focusing efficiency of metasurface array is very important as a means of WPT. A well-designed focusing transmission device can obtain high energy transmission efficiency. In the design of this paper, focusing efficiency η can be determined by the ratio of the total energy P_d of the focusing area at the reference plane and the total energy P_g of the entire focusing metasurface aperture, that is:

$$\eta = \frac{P_d}{P_g} \tag{4}$$

As shown in Figure 12, S_d and S_g are the area of the focusing aperture and the physical aperture of the reflective metasurface on the near-field observation plane, respectively. P_d and P_g can be calculated by numerical integration based on Poynting's theorem. The specific calculation formulas are as follows:

$$P_d = \int_{S_d} \mathrm{Re}(\overrightarrow{E} \times \overrightarrow{H}) \cdot d\overrightarrow{s}$$

$$P_g = \int_{S_g} \mathrm{Re}(\overrightarrow{E} \times \overrightarrow{H}) \cdot d\overrightarrow{s}$$

Through the CST full wave simulation, the values of P_d and P_g are calculated to obtain the focusing efficiency. Finally, the focusing efficiency of 7.25 GHz and 20 GHz is 56.9% and 57.5%, respectively, showing good focusing features. Under the corresponding operating frequency, the focusing energy of the metasurface designed in this paper in the focusing plane is better than that in the Reference [18].

5. CONCLUSIONS

Firstly, a new reflective metasurface element is proposed, which adopts a single-layer structure to reduce the design difficulty. The reflection coefficient phase is greater than 360° at 7.25 GHz and 20.5 GHz, meeting the design requirements. On the basis of completing the unit design, the array is assembled, and a dual frequency reflective metasurface is designed to focus at (0, 0, 200) mm. The focusing efficiency of 7.25 GHz and 20.5 GHz is calculated to be 56.9% and 57.5%, respectively, indicating that this research has potential application value in the field of WPT.

REFERENCES

1. Li, P., M. Lewin, A. V. Kretinin, et al., "Hyperbolic phonon-polaritons in boron nitride for near-field optical imaging and focusing," *Nature Communication*, Vol. 6, 7507, 2015.

2. Lipworth, B., J. Ensworth, K. Seetharam, et al., "Magnetic metamaterial superlens for increased range wireless power transfer," *Science*, Vol. 4, 3642, 2014.
3. Singh, R. K., A. Michel, P. Nepa, A. Salvatore, M. Terraroli, and P. Perego, "Compact and wearable Yagi-like textile antennas for near-field UHF-RFID readers," *IEEE Transactions on Antennas and Propagation*, Vol. 69, No. 3, 1324–1333, 2021.
4. Musavi, F. and W. Eberle, "Overview of wireless power transfer technologies for electric vehicle battery charging," *IEEE Power Electronics*, Vol. 7, No. 1, 60–66, 2014.
5. Sherman, K., "Properties of focused apertures in the Fresnel region," *IEEE Transactions on Antennas and Propagation*, Vol. 10, No. 4, 399–408, 1962.
6. Hansen, R. C., "Focal region characteristics of focused array antennas," *IEEE Transactions on Antennas and Propagation*, Vol. 33, No. 12, 1328–1337, 1985.
7. Shafai, L., A. A. Kishk, and A. Sebak, "Near field focusing of apertures and reflector antennas," *Communications, Power and Computing*, 246–251, 1997.
8. Bor, J., S. Clauzier, O. Lafond, and M. Himdi, "60 GHz foam-based antenna for near-field focusing," *Electronics Letters*, Vol. 50, No. 8, 571–572, 2015.
9. Buffi, A., P. Nepa, and G. Manara, "Design criteria for near-field-focused planar arrays," *IEEE Antennas & Propagation Magazine*, Vol. 54, No. 1, 40–50, 2012.
10. Tofigh, F., J. Nourinia, M. Azarmanesh, and K. M. Khazaei, "Near-field focused array microstrip planar antenna for medical applications," *IEEE Antennas and Wireless Propagation Letters*, Vol. 13, 951–954, 2014.
11. Siragusa, R., P. Lemaitre-Auger, and S. Tedjini, "Tunable near-field focused circular phase-array antenna for 5.8-GHz RFID applications," *IEEE Antennas and Wireless Propagation Letters*, Vol. 10, 33–36, 2011.
12. Stephan, K. D., J. B. Mead, D. M. Pozar, L. Wang, and J. A. Pearce, "A near field focused microstrip array for a radiometric temperature sensor," *IEEE Transactions on Antennas and Propagation*, Vol. 55, No. 4, 1199–1203, 2007.
13. Karimkashi, S. and A. A. Kishk, "Focusing properties of Fresnel zone plate lens antennas in the near-field region," *IEEE Transactions on Antennas and Propagation*, Vol. 59, No. 5, 1481–1487, 2011.
14. Luo, W. and L. Xu, "Wireless power transfer in the radiative near-field using a reconfigurable holographic metasurface aperture," *IEEE International Conference on Communications*, 1–5, 2018.
15. Wang, T., G. Zhai, R. Xie, et al., "Dual-band terahertz auto-focusing airy beam based on single-layer geometric metasurfaces with independent complex amplitude modulation at each wavelength," *Advanced Theory and Simulations*, 2019.
16. Li, J., Y. Yuan, Q. Wu, et al., "Dual-band independent phase control based on high efficiency metasurface," *Chinese Optics Letters*, Vol. 19, No. 10, 100501, 2021.
17. Wang, T., R. Xie, S. Zhu, et al., "Dual-band high efficiency terahertz meta-devices based on reflective geometric metasurfaces," *IEEE Access*, Vol. 7, 58131–58138, 2019.
18. Chia, T. T., T. K. Chua, and Z. N. Chen, "Design of a C-band reflectarray antenna for near-field applications," *International Conference on Electromagnetics in Advanced Applications*, 1028–1031, 2019.
19. Zhang, P., L. Li, X. Zhang, H. Liu, and Y. Shi, "Design, measurement and analysis of near-field focusing reflective metasurface for dual-polarization and multi-focus wireless power transfer," *IEEE Access*, Vol. 7, 110387–110399, 2019.
20. Zhang, N., K. Chen, W. Zhao, G. Qian, J. Zhao, and Y. Feng, "Reconfigurable coding metasurface for dual-band dynamic near-field microwave focusing," *International Conference on Microwave and Millimeter Wave Technology*, 1–3, 2020.
21. Zhang, P., L. Li, and Y. Liu, "A dual-band reflective metasurface using near-field focusing and zero-order bessel beam for wireless power transfer," *International Conference on Microwave and Millimeter Wave Technology*, 1–3, 2019.

22. Cui, X. W., M. Wang, M. Chang, P. Zhang, J. Chen, and L. Li, "Analysis of feed antenna in near-field focusing-based reflectarray for wireless power transfer," *IEEE MTT-S International Wireless Symposium*, 1–3, 2020.
23. Du, G., D. Wang, X. Sun, and Y. Zhao, "Design of a reflective metasurface for near-field focusing," *IEEE International Symposium on Antennas and Propagation and USNC-URSI Radio Science Meeting*, 323–324, 2021.